FUTURE MEDICINAL CHEMISTRY
2025, VOL. 17, NO. 10, 1105–1117
https://doi.org/10.1080/17568919.2025.2504337

Taylor & Francis
Taylor & Francis Group

RESEARCH ARTICLE

Check for updates

Benzothiazole derivatives as inhibitors of chikungunya virus replicative cycle

Shiraz Feferbaum-Leite[a], Natasha Marques Cassani[a], Uriel Enrique Aquino Ruiz[a], Renieidy Flávia Clemente Dias[b], Danilo Nascimento Farago[b], Marco Guevara-Vega[c], Nilson Nicolau-Junior[d], Robinson Sabino-Silva[c], Celso de Oliveira Rezende Júnior[b] and Ana Carolina Gomes Jardim[a,e]

[a]Laboratory of Antiviral Research (LAPAV), Institute of Biomedical Science (ICBIM), Federal University of Uberlândia (UFU), Uberlândia, Minas Gerais, Brazil; [b]Drug Candidate Synthesis Laboratory (LaSFar), Institute of Chemistry, Federal University of Uberlândia (UFU), Uberlândia, Minas Gerais, Brazil; [c]Innovation Center in Salivary Diagnostic and Nanobiotechnology, Department of Physiology, Institute of Biomedical Sciences, Federal University of Uberlandia, Uberlandia, Minas Gerais, Brazil; [d]Institute of Biotechnology, Federal University of Uberlândia (UFU), Uberlândia, Minas Gerais, Brazil; [e]Institute of Biosciences, Humanities and Exact Sciences (Ibilce), São Paulo State University (Unesp), São José do Rio Preto, São Paulo, Brazil

ABSTRACT

Aims: Chikungunya virus (CHIKV) is the agent of chikungunya fever (CHIKF), a reemerging disease prevalent in tropical regions. With no licensed treatments available, identifying effective antiviral compounds is critical. This study evaluates the antiviral potential of 20 synthetic sulfonamide derivatives against CHIKV.

Methodology: We tested 13 heteroaromatic derivatives containing thiazole, benzimidazole, and benzothiazole (BTA) moieties, along with seven sulfonamides bearing ester and carboxylic acid groups. CHIKV-*nanoluc* replication was assessed *in vitro*, and molecular docking and infrared spectroscopy studies were conducted to explore interactions with viral proteins.

Results: BTA derivatives 6, 9, 11, and 13 demonstrated potent CHIKV inhibition, with EC_{50} values between 14.9 and 63.1 µM and selective indexes of 13.8, 5.8, 4.4, and 11, respectively. All compounds acted in the virus post-entry stage, with compound 9 reducing viral replication by 98%. Compound 9 exhibited multi-stage activity, inhibiting CHIKV through virucidal (55%), pre-treatment (69%), and entry (98%) mechanisms. Molecular docking suggested strong binding affinities to CHIKV non-structural proteins and envelope glycoproteins. Infrared spectroscopy corroborated compound 9's interaction with the glycoprotein complex and lipids.

Conclusions: These findings highlight BTA derivatives as promising CHIKV inhibitors. Compound 9's ability to interfere at multiple stages of infection suggests its potential for therapeutic development against CHIKF.

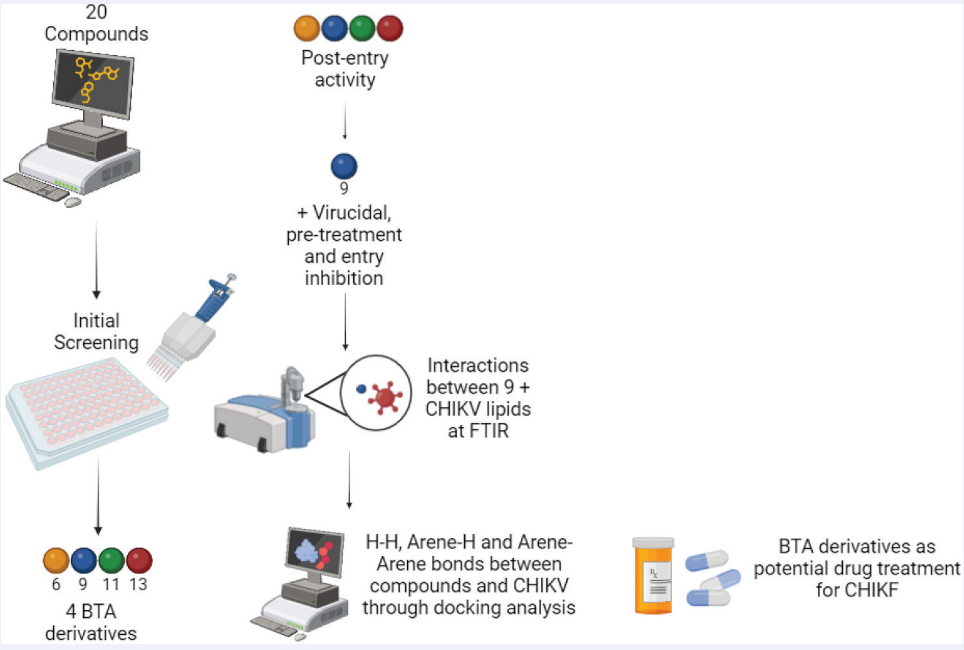

ARTICLE HISTORY

Received 17 January 2025
Accepted 28 April 2025

KEYWORDS

Chikungunya virus; sulfonamide; carboxylic acid; thiazole; benzimidazole; benzothiazole

CONTACT Ana Carolina Gomes Jardim jardim@ufu.br Institute of Biomedical Science (ICBIM), Federal University of Uberlândia (UFU), Avenida Amazonas, 4C Room 216, Umuarama, Uberlândia, Minas Gerais 38405-302, Brazil

Supplemental data for this article can be accessed online at https://doi.org/10.1080/17568919.2025.2504337

© 2025 Informa UK Limited, trading as Taylor & Francis Group

Article highlights

- Benzothiazole (BTA) derivatives impair CHIKV replication.
- BTA moiety might be responsible for the inhibitory effect on post-entry stage of CHIKV replication.
- Compound 9 inhibits multiple stages of CHIKV replicative cycle.
- Molecular docking analysis suggests strong H–H, arene-H, and arene–arene bonds of envelope glycoproteins with BTA compounds.
- ATR-FTIR indicates interactions between BTA derivatives and CHIKV envelope lipids.

1. Introduction

Chikungunya virus (CHIKV) is an enveloped arbovirus, belonging to the *Alphavirus* genus and *Togaviridae* family, transmitted by the female bite of *Aedes aegypti* or *Aedes albopictus* in urban cycles [1]. CHIKV exhibits a single-stranded positive-sense RNA with a 11.8 kb genome consisting of two open reading frames (ORF), one that encodes four non-structural proteins (nsP1, nsP2, nsP3, and nsP4), and the second that encodes five structural proteins (C – capsid; 6K/TF – transframe; E1/E2/E3 – envelope glycoprotein) [2].

Responsible for triggering chikungunya fever (CHIKF), CHIKV has been a global health problem, mainly in the Americas, Africa, and some regions of Asia due to the tropical climate favorable to the development of mosquito reservoirs [3]. The illness may lead to chronic complications, such as severe arthritis, limiting the quality of life of infected individuals [4].

Currently, there is no licensed drug to treat CHIKF, restricting medical management to medications that alleviate the symptoms. In this context, novel compounds can be synthesized based on organic scaffolds to enhance and target their pharmacological properties, leading to the development of effective and safe drugs for a wide range of treatments [5,6]. Sulfonamide exemplifies a structure present in biologically active compounds, including antibiotics, antihypertensive agents, and antithyroid medications [7]. Furthermore, this group encompasses some commercialized drugs involved in enzyme inhibition like Amprenavir, which is a protease inhibitor of human immunodeficiency virus (HIV), and Sulthiame, employed as an anticonvulsant that acts as carbonic anhydrase enzyme inhibitor [8]. In medicinal chemistry, sulfonamide moiety can be applied as a bio isostere for the carboxylic acid group, as it is capable of forming the same hydrogen bonds and its oxygen atoms are positioned at similar distances [9]. This exchange can avoid some disadvantages of the carboxylic group, such as toxicity, metabolic instability, and limited passive diffusion in biological membranes [10].

Alternatively, benzothiazole (BTA) possesses a chemical structure composed of oxygen, nitrogen, and sulfur, where its nucleus is formed by a fusion of thiazole and benzene rings [11]. It is rarely found in some natural products like the compound produced by *Aspergillus clavatus*, cranberries aroma, and fermentation culture extracts of *Micrococcus* sp., a marine bacterium [12]. Due to versatile manipulation in various ring positions, their derivatives have gained attention as optimized drug candidates [13]. A plethora of BTA derivatives have demonstrated broad-spectrum biological activity, such as antitumor [14], anti-diabetic [15], analgesic [16], anti-parasitic [17], and antibacterial [18]. In addition, antiviral activities against herpes simplex virus (HSV) [19], influenza A virus [20], and dengue virus (DENV) [21] have also been described.

The association between sulfonamides and heterocycle compounds like BTAs has been recently described as molecular hybrids, which is the union of two or more pharmacophores in a scaffold [22]. Considering the number of biological activities displayed by both, this may lead to synergistic pharmacological activities and an increased ability to bind to more than one target [23].

Given the previously reported inhibitory effects of these sulfonamide derivatives against ZIKV [24], we sought to investigate their potential antiviral activity against CHIKV *in vitro*. Since ZIKV and CHIKV are both arboviruses and share aspects of their replication mechanisms, we hypothesized that these compounds could exhibit a broader antiviral spectrum. By evaluating their effects on CHIKV, we aim to identify promising candidates that could serve as antiviral agents against multiple arboviruses, particularly those of public health concern. Our findings may highlight the potential of BTA derivatives (heteroaromatic insertions) as a valuable scaffold for antiviral drug development.

2. Materials and methods

2.1. Compounds

All the sulfonamides were synthesized as previously reported [17,24]. The 20 compounds evaluated in this work were divided into two classes. Figure 1(b) shows the chemical structure of the 13 representative heteroaromatic sulfonamide compounds, except for compound **13**, which is not a sulfonamide, but rather a simplified derivative of BTA with an *N*-acetyl amino fragment. These 13 compounds are divided into three subclasses, where **1–2** are thiazole derivatives, **3** is a benzimidazole derivative, while compounds **4–13** are BTA derivatives. Figure 1(c) shows the chemical structure of the seven representative carboxylic acid-derived sulfonamide compounds.

Compounds were dissolved in dimethyl sulfoxide (DMSO, Labsynth, Brazil) and stored at −20ºC in 50 mm stock solutions. Dilutions of compounds in cell culture medium were performed immediately prior to the assays to a final concentration of DMSO of 0.1%.

2.2. Cell culture

BHK-21 cells (fibroblasts derived from Syrian golden hamster kidney; ATCC® CCL-10™, used between passages 15 and 25) were maintained in Dulbecco's modified Eagle's medium (DMEM, Sigma-Aldrich) supplemented with 100 U/mL of penicillin (Hyclone Laboratories), 100 mg/mL of streptomycin (Hyclone Laboratories), 1% dilution of non-essential amino acids (Hyclone Laboratories), and 5% of fetal bovine serum (FBS, Hyclone Laboratories) in a 5% CO_2 incubator at 37°C.

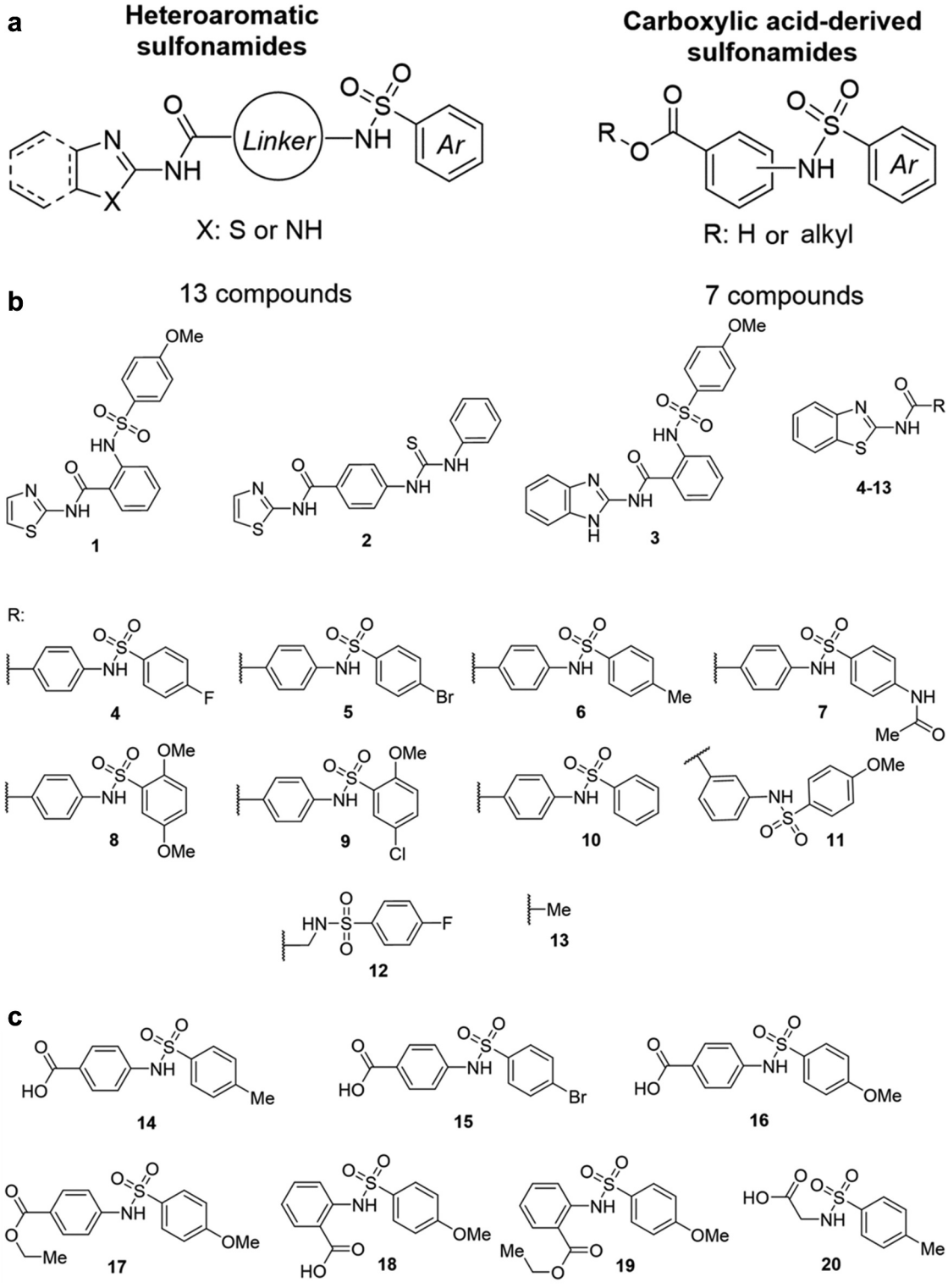

Figure 1. Chemical structures of the compounds. (a) General chemical structure of the compounds investigated in this work [24]. (b) Representative heteroaromatic sulfonamide compounds [24]. (c) Representative carboxylic acid-derived sulfonamide compounds [24].

2.3. Virus sample

The CHIKV-expressing nanoluciferase reporter (CHIKV-*nanoluc*) used for the antiviral assays is based on the CHIKV isolate LR2006OPY1 (East/Central/South African genotype) [25]. This construct was produced, rescued, and titrated as previously described [26].

2.4. Cell viability and determination of the cytotoxic concentration of 50% (CC_{50})

Cell viability was measured by MTT [3-(4,5-dimethylthiazol-2-yl)-2,5-diphenyl tetrazolium bromide, Sigma-Aldrich] assay. For screening assays, BHK-21 cells were plated into 96 well plates at a density of 2×10^4 cells per well and incubated

overnight at 37°C. Medium containing each compound at 50 and 10 µM was added, and cells were incubated for 24 h. DMSO 0.1% was used as an untreated control. After this, the medium was replaced with the MTT solution at 1 mg/mL, cells were incubated for 30 min, after which the MTT solution was removed and replaced with 100 µL of DMSO (Labsynth, Brazil) to solubilize the formazan crystals. The absorbance was measured at 560 nm on the Glomax microplate reader (Promega, USA). Cell viability was calculated according to the equation (T/C) × 100%, where T and C represent the mean optical density of the treated and untreated control groups, respectively.

For determination of the cytotoxic concentration of 50% (CC_{50}), BHK-21 cells were plated to 48 well plates at a density of 5×10^4 cells per well and incubated overnight at 37°C. Medium containing two-fold serial dilutions at concentrations ranging from 1.6 to 200 µM for **6**, **9**, **11** and from 3.1 to 400 µM for **13** was added to cells and incubated for 16 h. Subsequently, the medium was replaced by MTT solution at 1 mg/mL and proceeded as described above. CC_{50} was calculated using nonlinear regression in GraphPad Prism 8.0.

2.5. Antiviral activity and determination of the effective concentration of 50% (EC_{50})

To assess the antiviral activity of the compounds, BHK-21 cells were seeded at a density of 5×10^4 cells per well into 48 well plates 24 h before the assays. Cells were infected with CHIKV-*nanoluc* at a multiplicity of infection (MOI) of 0.1 for antiviral trials in the presence of the compounds at the highest non-cytotoxic concentration analyzed through the cell viability assay. DMSO 0.1% was used as an untreated control. Samples were harvested using Passive Lysis Buffer (Promega, USA) at 16 h post-infection (h.p.i.), and virus replication levels were quantified by measuring nanoluciferase activity using the *Renilla* Luciferase Assay System (Promega, USA) at Glomax microplate reader (Promega, USA). Data were calculated according to the equation (T/C) × 100%, where T and C represent the mean of luminescence signals of the treated and untreated control groups, respectively.

Similar to CC_{50}, EC_{50} assays were conducted through the treatment of cell with two-fold serial dilutions of the compounds, at concentrations ranging from 1.5 to 200 µM for **6**, **9**, **11** and from 3.1 to 400 µM for **13** in the presence of CHIKV-*nanoluc* at a MOI of 1. Concentrations were defined based on the cytotoxicity assays. EC_{50} was calculated using nonlinear regression in GraphPad Prism 8.0. The values of CC_{50} and EC_{50} were used to calculate the selectivity index ($SI = CC_{50}/EC_{50}$).

All the infection assays were performed at a BSL-2 laboratory under the authorization number CBQ: 163/02 and process SEI: 01.245.006267/2022–14 from the CTNBio – National Technical Commission for Biosecurity from Brazil.

2.6. Time-of-drug-addition assays

For all the time-of-drug-addition assays, BHK-21 cells at 5×10^4 cells per well were seeded in 48 well plates 24 h before infection and treatment. Compounds **6**, **9**, and **11** were evaluated at 10 µM, whereas **13** was at 50 µM, determined at viability screening as the highest non-cytotoxic concentrations. All infections were performed at MOI of 1, except for the virucidal protocol (MOI = 5). The efficiency of virus replication was assessed by measurement of nanoluciferase activity at 16 h.p.i using the *Renilla*-luciferase assay system (Promega, USA).

In the pretreatment assay, cells were treated for 1 h with compounds prior to the infection, extensively washed with phosphate-buffered saline (PBS) [1×], and added of CHIKV-*nanoluc* for 1 h. Then, cells were washed with PBS [1×] to remove unbound virus and added to DMEM 2%. In the entry inhibition assay, cells were infected using media containing the compound and virus for 1 h, washed with PBS [1×] and incubated with fresh medium. The virucidal activity was assessed using the same setting, except that the inoculum containing compound and virus were incubated for 1 h before it was added to the cells. Finally, in the post-entry assay, cells were infected with CHIKV-*nanoluc* for 1 h, washed extensively with PBS [1×], and then incubated in a compound-containing medium for 16 h. DMSO 0.1% was used as untreated control for all protocols. Data were calculated according to the equation (T/C) × 100%, where T and C represent the mean of luminescence signals of the treated and untreated control groups, respectively.

2.7. Molecular docking

Structures of nsPs 1, 2, 3 and the envelope glycoprotein complex (E1E2E3) of CHIKV were obtained from Protein Data Bank (PDB) from the entries 7X01, 3TRK, 6W0T, and 3N42, respectively. The nsP4 structure was obtained by *in silico* modeling using AlphaFold2 (ColabFold v1.5.5, UK) [27]. Potential binding sites were predicted by the SiteFinder MOE tool (Chemical Computing Group, Canada) for all proteins. The compounds **6**, **9**, **11**, and **13** were docked to all nsPs using the MOE (2024) program. All proteins were submitted to MOE QuickPrep (Chemical Computing Group, Canada) to correct structural problems. Molecular docking was performed using the Triangle Matcher placement method (30 poses) and London dG as the scoring function. Refining was conducted using an induced fit with GBVI/WSA dG as a scoring function. The best GBVI/WSA dG ranked was selected by each complex for the 3D and 2D analysis. 3D images were generated by MOE and ChimeraX (RBVI, USA) [28] programs and 2D images were generated by MOE.

2.8. Infrared spectral data analysis

The infrared spectra of the samples (CHIKV, the compound **9**, and the combination of CHIKV + 9) were recorded using Attenuated Total Reflectance-Fourier Transform Infrared (ATR-FTIR) spectroscopy with the Agilent Cary 630 FTIR (Agilent Technologies, USA). For this analysis, the lipidic region (3050–2800 cm^{-1}) and the fingerprint region (1800–800 cm^{-1}) were examined. The samples were prepared separately with the compound **9** and/or CHIKV [29,30]. A volume of 3 µL from each sample was placed on

the diamond cell, forming a thin layer on the ATR crystal. The spectra were recorded at a resolution of 2 cm^{-1} with 64 scans. The second derivative spectra were derived from the original data and plotted using Origin Pro 9.8.0.200 software (OriginLab, USA). The second derivative was applied to correct baseline drifts and to improve the resolution of overlapping spectral peaks [31]. The second derivative spectra enable more precise identification of subtle and adjacent absorption vibrational modes which are not resolved in the original spectrum, thereby improving the specificity of absorption vibrational modes for certain molecules [31]. Adjustments were made using the Savitzky–Golay algorithm with a polynomial order of 2 and a 20-point window [30,32]. The tentative assignments were derived from infrared spectra in biological tissues [33].

2.9. Statistical analysis

Individual experiments were performed in triplicates, and all assays were performed a minimum of three times to confirm the reproducibility of the results. GraphPad Prism 8.0 software was used to assess normal distribution and statistical differences of means. $p < 0.05$ values (indicated by asterisks) were considered statistically significant. For the establishment of CC_{50} and EC_{50} values, the data were transformed into log(X), where X is the concentration, and submitted into a non-linear regression log(inhibitor) vs. response with four parameters in variable slope.

3. Results

3.1. Design and synthesis of compounds

To identify compounds with superior anti-CHIKV activity, two classes of sulfonamide derivatives (heteroaromatic sulfonamides and carboxylic acid-derived sulfonamides) were designed, synthesized, and evaluated. The design strategy emphasized chemical diversification to explore a broad structural space. The heteroaromatic sulfonamide class was developed with variations in the heteroaromatic fragment, including thiazole, benzimidazole, and benzothiazole derivatives, alongside modifications to the benzenesulfonyl ring substituents, incorporating groups with diverse electronic and steric effects. Similarly, the carboxylic acid-derived sulfonamide class was designed with various substitutions on the benzenesulfonamide ring, encompassing both free carboxyl and ester derivatives. Design and synthesis were conducted according to Supplementary material and as previously described [24]. This array of structural modifications aimed to modulate compound interactions with CHIKV, leading to varied inhibition profiles.

3.2. Antiviral activity of sulfonamide compounds against CHIKV

To assess the antiviral effect of the sulfonamide derivatives, the cytotoxicity of these compounds was first investigated. To this, BHK-21 cells, a well-established model for CHIKV that supports efficient replication and quantification, were treated with each compound at concentrations of 50 and 10 µM. Analyzing the effect on cell viability, we found that treatment with the heteroaromatic sulfonamide compounds **2**, **8,** and **13** at 50 µM presented no significant cytotoxicity ($p = 0{,}6865$, $p > 0{,}9999$ and $p = 0{,}9988$, respectively) (Figure 2(a)). At 10 µM, all the compounds were viable to the cells, except for **4** (81%; $p = 0.0282$), **5** (56%; $p < 0.0001$), and **10** (69%; $p < 0.0001$) (Figure 2(a)).

For the carboxylic acid-derived sulfonamide group, only **14** (81%; $p = 0.0210$) and 20 (80%; $p = 0.0262$) were viable to the cells at 50 µM (> 80%), while the others were viable at 10 µM (Figure 2(b)). With an exception, compounds **15** (50 µM – 74% - $p = 0.0002$; 10 µM – 80% - $p = 0.0099$) and **17** (50 µM – 79% - $p = 0.0132$; 10 µM – 74% - $p = 0.0011$) demonstrated to be cytotoxic at both concentrations (Figure 2(b)).

Then, BHK-21 cells were infected with CHIKV-*nanoluc* at MOI of 0.1 and treated with the compounds at the highest non-cytotoxic concentration to evaluate their antiviral activity. For compounds that showed cytotoxicity at 50 and 10 µM, such as **4**, **5**, **10**, **15,** and **17**, antiviral assay was performed at 2 µM. Viability assay was performed in parallel for all compounds.

All the compounds from heteroaromatic sulfonamide group showed significant inhibition of CHIKV replication ($p < 0{,}0001$), where BTA derivatives **6** (90%), **9** (95%), **11** (98%), and **13** (94.5%) presented the strongest antiviral effects, highlighting their potential as promising scaffolds for the development of CHIKV antiviral drugs (Figure 2(c)). On the other hand, none of the carboxylic acid-derived sulfonamide compounds were capable of inhibiting CHIKV infection above 80%. Compounds **16**, **17,** and **19** presented inhibition rates between 12% and 72% ($p < 0.01$) (Figure 2(d)).

3.3. BTA derivatives of sulfonamide groups possess robust response against CHIKV in vitro

From screening tests, the compounds with inhibition over 80% (**6**, **9**, **11**, and **13**) were selected for further evaluation. The effective concentration of 50% (EC_{50}), cytotoxic concentration of 50% (CC_{50}), and selective index ($SI = CC_{50}/EC_{50}$) were determined. Compounds **6** and **9** demonstrated, respectively, EC_{50} of 14.9 µM and 17 µM, CC_{50} of 205.2 µM and 97.9 µM, and a SI of 13.8 and 5.8 (Figure 3(a,b)). While **11** and **13** showed, in this order, EC_{50} of 63.1 µM and 41.6 µM, CC_{50} of 276 µM and 459.3 µM, and SI of 4.4 and 11.0, respectively (Figure 3(c,d)).

3.4. BTA derivatives reveal strong post-entry activity, with a multiple effect of compound 9

As shown in Figure 4, time-of-drug-addition assays were carried out for **6**, **9**, **11**, and **13** to further investigate the effects of these compounds on different stages of CHIKV replicative cycle. For this, BHK-21 cells were infected with CHIKV-*nanoluc* at a MOI of 5 for the virucidal test and a MOI of 1 for the pretreatment, entry, and post-entry stages, and the compounds were added to the cells as described in methods. Interestingly, the results demonstrated that **9** inhibited all stages of replicative cycle investigated, showing 55% of inhibition at virucidal test, 69% at pretreatment, 79% at entry stage, and 98% at post-entry

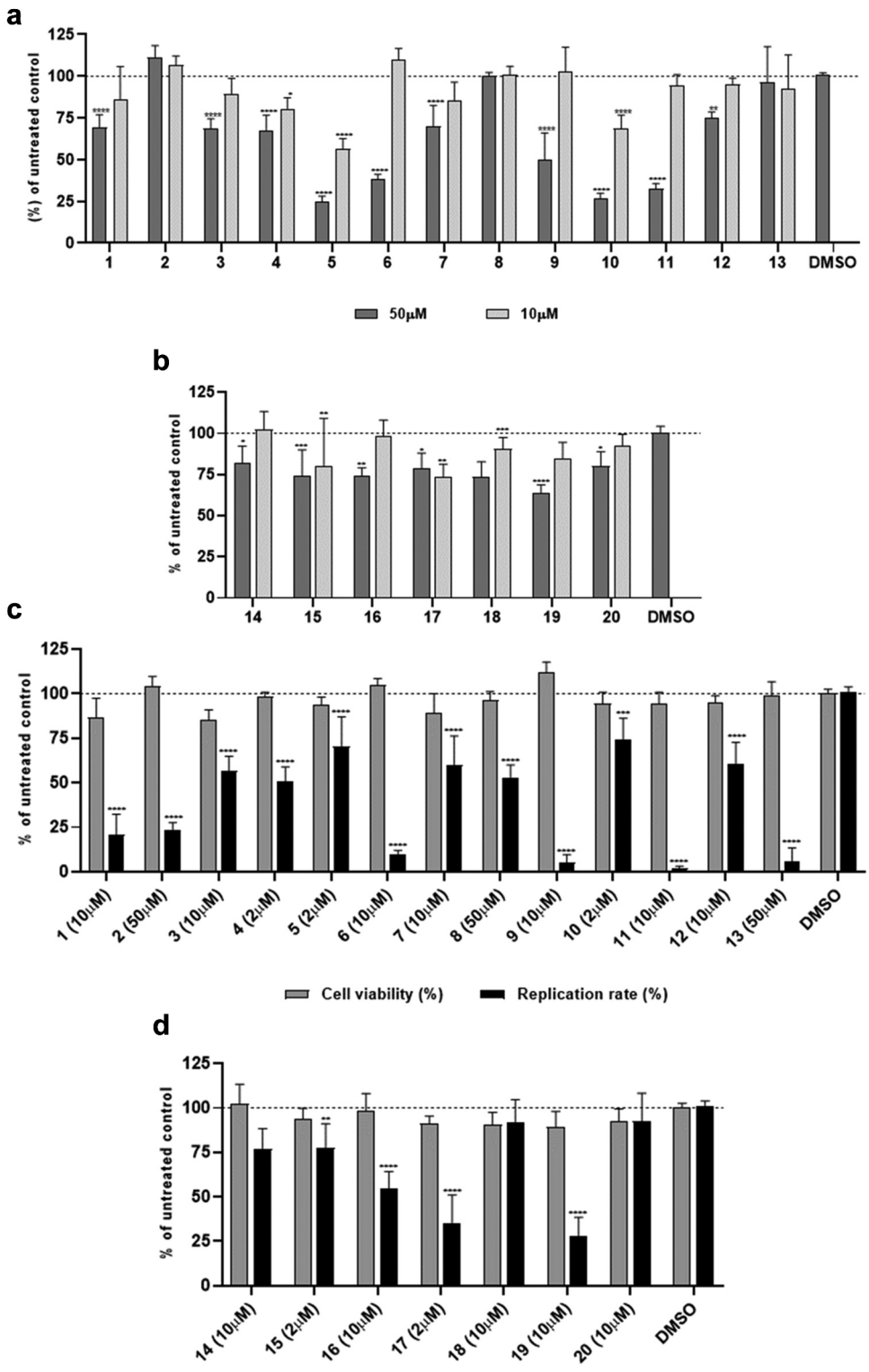

Figure 2. Effect of sulfonamide compounds on BHK-21 viability and CHIKV-*nanoluc* infection. Cell viability was accessed by treating BHK-21 cells with (a) heteroaromatic sulfonamide compounds, in which 1–3 are thiazole and benzimidazole derivatives and 4–13 are BTA derivatives; and (b) carboxylic acid-derived sulfonamide compounds, at 50 and 10 µM. After treatment, the medium with compound was removed and replaced by fresh medium with MTT at 1 mg/mL and incubated for 30 min. After incubation, medium was removed, and the crystals solubilized with DMSO. Surviving cells were measured by absorbance (560 nM). For antiviral assays, BHK-21 cells were infected with CHIKV-nanoluc at an MOI of 0.1 and simultaneously treated with (c) heteroaromatic sulfonamides and (d) carboxylic acid-derived sulfonamide group, at the highest non-cytotoxic concentration. After 16 h.p.i, cells were lysed, and a Renilla-luciferase assay was performed to assess CHIKV replication rates. Mean values of three independent experiments each measured in quadruplicate including the standard deviation are shown. DMSO 0.1% was used as an untreated control. p values < 0.05 were considered significant. (*) p <0.05; (**) p <0.01; (***) p <0.001; and (****) p <0.0001.

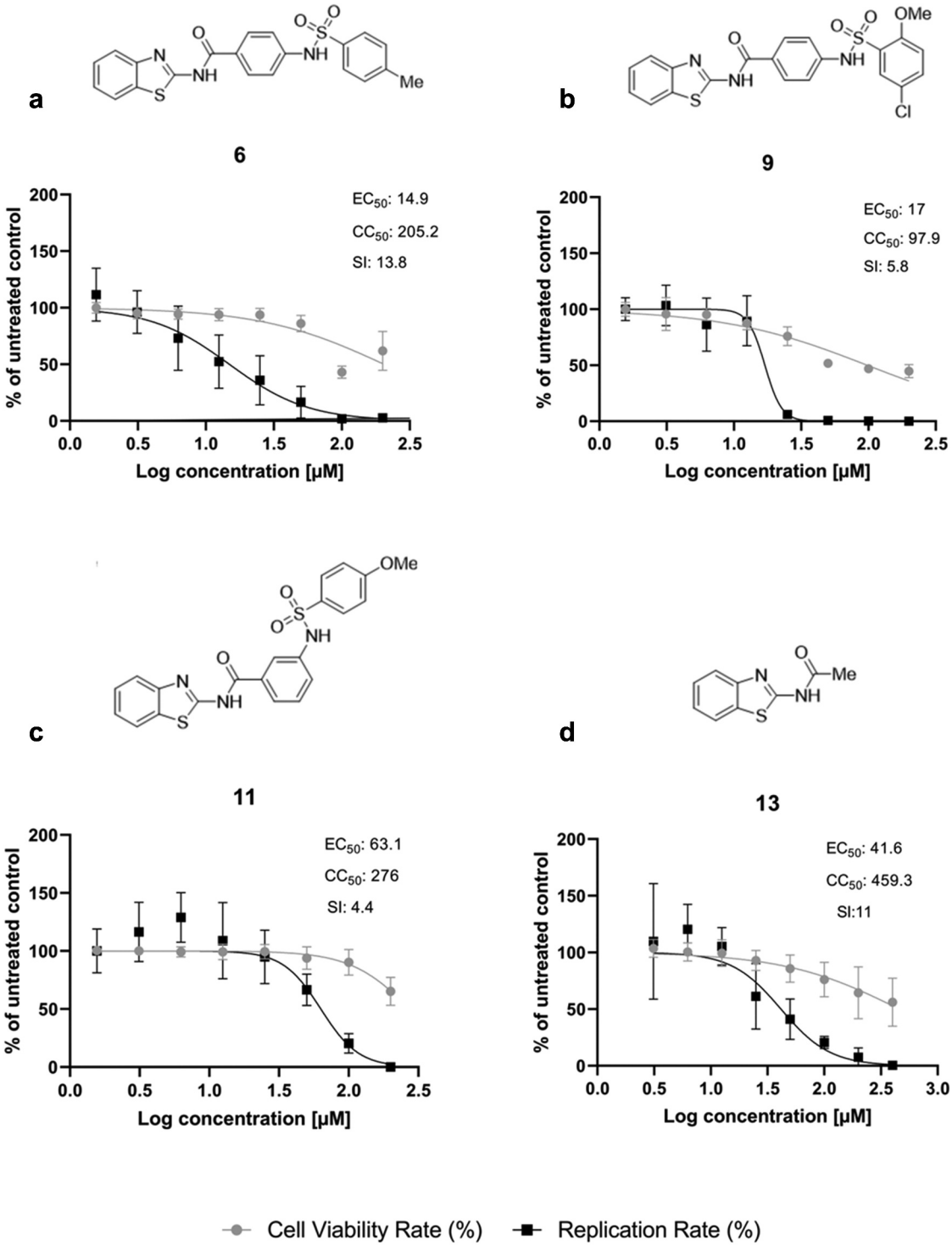

Figure 3. Dose-response curve of the compounds with highest rates of inhibition of CHIKV replication. BHK-21 cells were treated with compounds 6 (a), 9 (b), 11 (c), and 13 (d) at concentrations ranged from 1.6 to 200 μM, except for 13, which ranged from 3.1 to 400 μM. CHIKV replication was quantified by measuring nanoluciferase activity (black squares) and cell viability was measured using an MTT assay (gray dots). The mean values of three independent experiments each measured in triplicates, including the standard deviation, are shown. All images were generated using GraphPad prism 8.0 applying a nonlinear regression.

stage (Figure 4(a–d)). Compounds **11** and **13** were capable to significantly inhibit entry ($p < 0.05$) (Figure 4(c)) and post-entry stages ($p < 0.0001$) (Figure 4(d)), presenting stronger effect after viral entry to the host cells. Alternatively, compound **6** reduced 54% of viral post-entry to the host cells ($p < 0.0001$) (Figure 4(d)).

3.5. Insights on the molecular interactions between BTA derivatives and CHIKV proteins

According to the time-of-drug-addition assays, the four tested compounds demonstrated post-entry activity. Therefore, molecular docking calculations were performed with all CHIKV non-structural proteins. 2D diagrams and 3D images

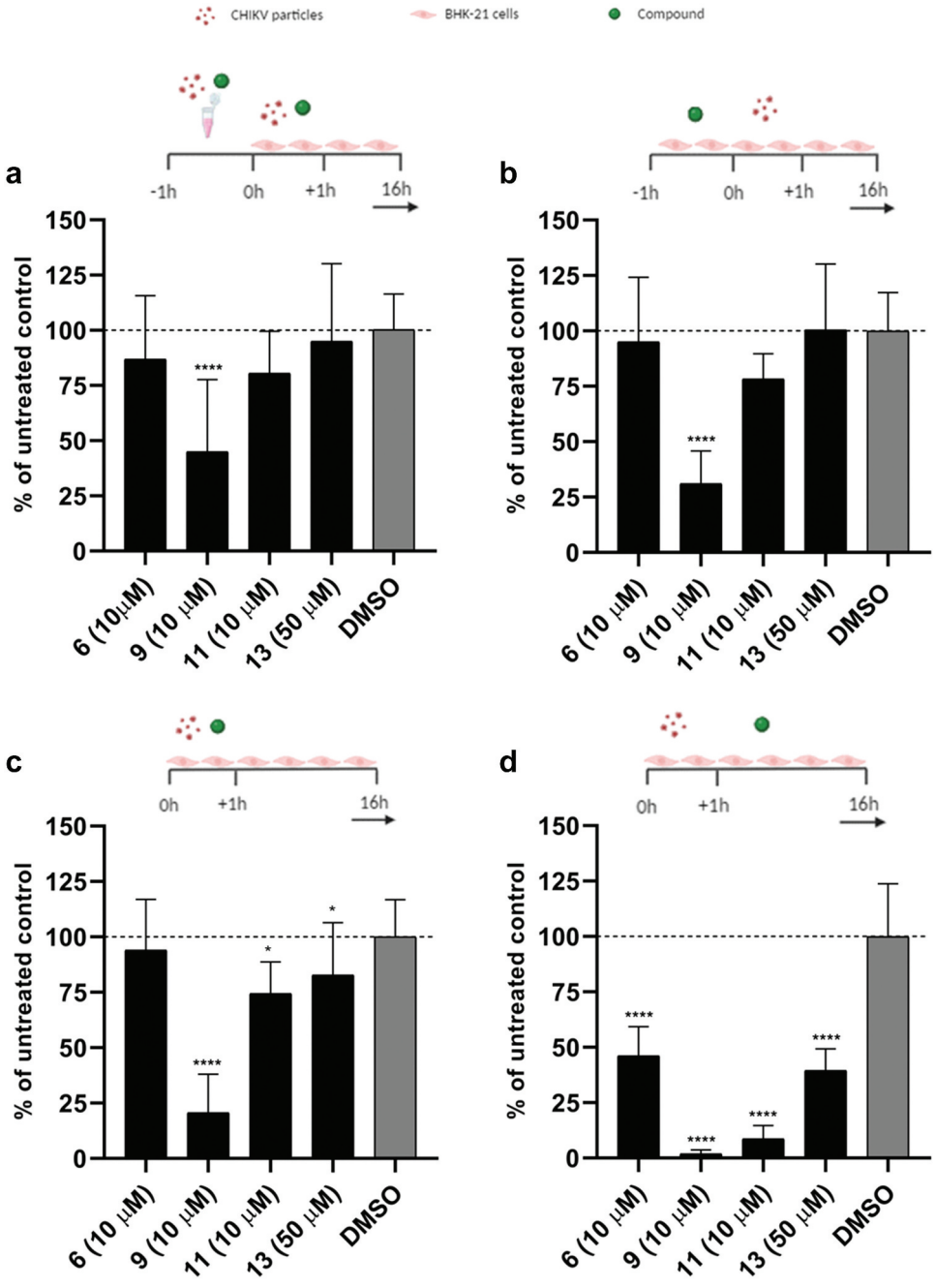

Figure 4. BTA derivatives activity on different stages of CHIKV-*nanoluc* replicative cycle. (a) Virucidal. BTA derivatives and CHIKV-*nanoluc* (MOI of 5) were incubated for 1 h. Then, the inoculum was added to the cells for an additional hour. Cells were washed and fresh medium was added. (b) Pre-treatment. BHK-21 cells were treated with the compounds for 1 h, cells were washed to remove compounds and were infected with CHIKV-*nanoluc* at MOI of 1 for 1 h. Then, the medium was removed, cells were washed to remove unbound virus, and a fresh medium was added. (c) Entry. BHK-21 cells were infected with CHIKV-*nanoluc* (MOI of 1) and simultaneously treated with the compounds for 1 h. Subsequently, cells were washed, and a fresh medium was added. (d) Post-entry. BHK-21 cells were infected with CHIKV-*nanoluc* (MOI of 1) for 1 h, cells were washed with PBS to remove unbound virus and treated with the respective derivatives. All infection assays were quantified 16 h.p.i through the measurement of luminescence levels. DMSO 0.1% was used as an untreated control. Mean ± SD values of a minimum of three independent experiments, each measured in triplicate. p values <0.05 were considered significant. (*) p <0.05; (**) p <0.01; (***) p <0.001; and (****) p <0.0001. A schematic representation of each time-based assay is indicated above in each graphic. Images were generated using GraphPad prism 8.0 and BioRender.

Table 1. Molecular docking scores between BTA derivatives and nonstructural and structural proteins of CHIKV.

	GBVI/WSA dG (kcal/mol)				
Compounds	nsP1	nsP2	nsP3	nsP4	Glycoproteins (E1-E2-E3)
6	−7.60	−7.35	−7.55	b > −7.97	*
9	−7.70	−7.63	b > −8.28	−7.38	b > −8.01
11	b > −8.06	−7.90	−7.80	−8.00	*
13	−5.35	b > −5.42	−5.33	−5.28	*

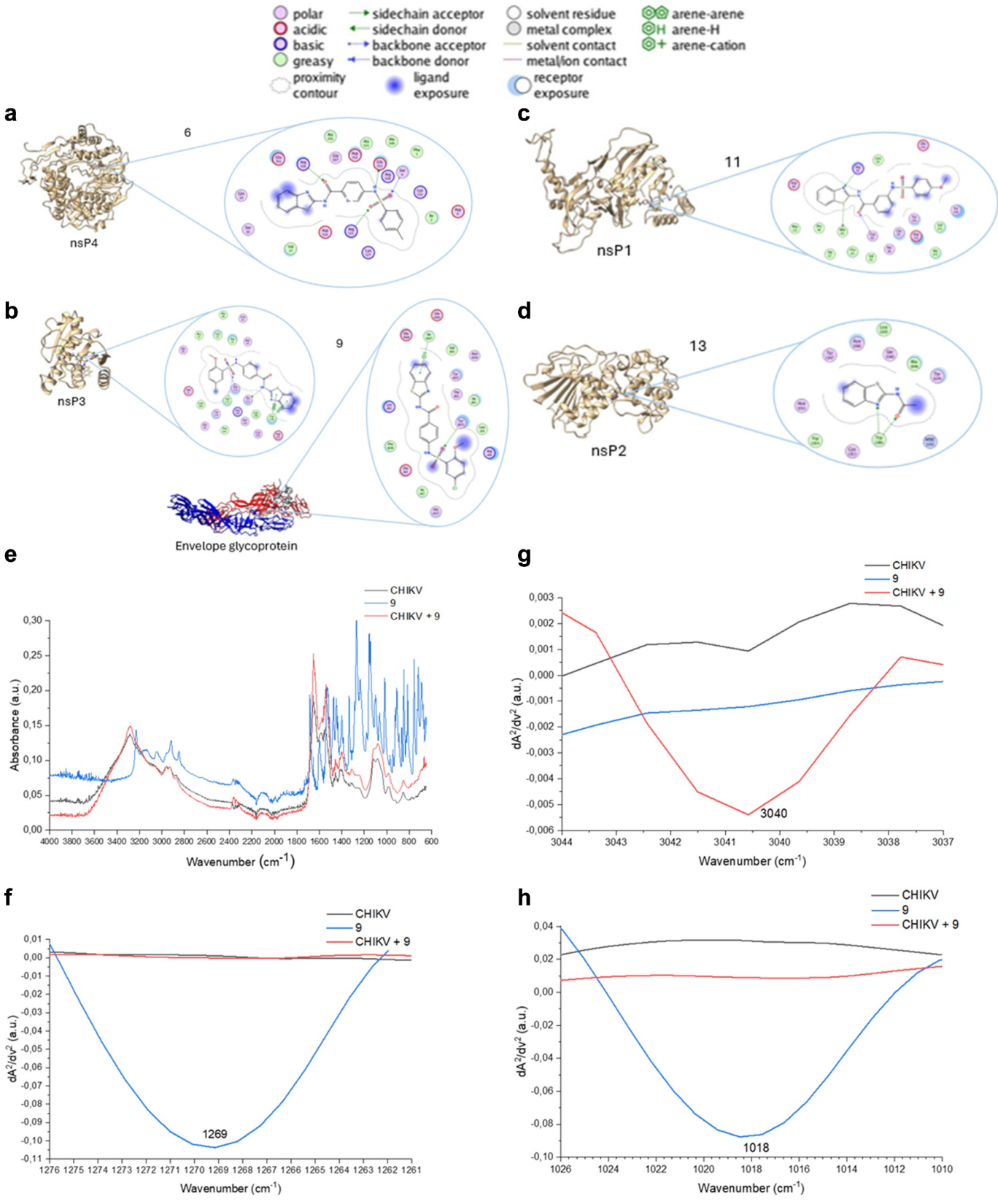

Figure 5. 2D and 3D and infrared spectroscopy interactions between BTA derivatives and CHIKV proteins are shown by molecular docking analysis. (a) **6** and nsP4 interact mostly through four hydrogen bonds with Arg521, Arg556, Glu553, and Ser4. (b) **9** exhibited three hydrogen bonds (Val113, Gly112, and Thr111) and two arene–arene bonds between Trp148 with nsP3; and one hydrogen bond (with Tyr233 from E2) and one arene-H bond (with Ile167 from E1) were identified with the glycoprotein complex. The blue chain represents E1; red represents E2; and gray represents E3. (c) **11** showed strong molecular interactions with nsP1 by three hydrogen bonds with residues Cys82, Met84, and Arg92. NsP4 structure was obtained by *in silico* modeling using AlphaFold2. (d) **13** revealed two hydrogen bonds with Trp1084 from nsP2. NsP1, 2, 3 and the envelope glycoprotein complex (E1E2E3) structures were obtained from protein data bank (PDB) from the entries 7X01, 3TRK, 6W0T, and 3N42, respectively. (e) Representative scheme of the ATR-FTIR technology with CHIKV-*nanoluc* (black line), the compound 9 (blue line), compound 9 plus CHIKV-*nanoluc* (red line). The original spectra are depicted in panel (e). Panels (f, g, h) depict the second-derivative spectra of vibrational modes at 3040, 1269, and 1018 cm^{-1}, respectively.

were generated to illustrate the optimal interactions exhibited by **6**, **9**, **11**, and **13** with the CHIKV proteins (Figure 5).

Compound **6** exhibited the most favorable docking GBVI/WSA dG score (indicative of the lowest binding energy in kcal/mol) for nsP4 (−7.97) among the other docked proteins, resulting in the formation of four hydrogen bonds with Arg521, Arg556, Glu553, and Ser4 (Table 1; Figure 5(a)). Concerning **9**, the best score was obtained by the nsP3 (−8.28), with interactions involving three hydrogen bonds (Val113, Gly112, and Thr111) and two arene–arene bonds with Trp148 (Table 1; Figure 5(b)). The interactions between **11** and nsP1 were characterized by three hydrogen bonds with residues Cys82, Met84, and Arg92 (Figure 5(c)). Compound **13** showed its highest docking score with the nsP2 protein (−5.42) and two hydrogen bonds with Trp1084 (Table 1; Figure 5(d)).

Furthermore, as **9** also demonstrated virucidal and entry activity, docking analysis was performed between this compound and the envelope glycoprotein complex, to better understand the molecular interactions involved. Regarding the envelope complex, compound **9** demonstrated a score of −8.01, where one hydrogen bond (with Tyr233 from E2) and one arene-H bond (with Ile167 from E1) were identified (Table 1; Figure 5(b)).

3.6. Infrared spectroscopy suggests interactions of compound 9 with CHIKV particles

The infrared spectra of the compound **9**, CHIKV-*nanoluc*, and compound **9** plus CHIKV-*nanoluc* are represented in Figure 5. The vibrational modes in CHIKV-*nanoluc* can be related to lipids, proteins, carbohydrates, and nucleic acids. The spectra of compound **9** also expressed several vibrational modes in the fingerprint region between 1800 and 600 cm^{-1}. The second derivative spectrum of the CHIKV-*nanoluc* associated with compound 9 at 3040 cm^{-1} revealed an additional vibrational mode that was absent in the spectra of compound **9** or CHIKV-*nanoluc* alone, suggesting interactions between the compound 9 and virus related to C–H stretching vibrations in lipids. Furthermore, vibrational modes at 1269 cm^{-1} and 1018 cm^{-1}, which were present in the spectrum of compound **9** alone, were absent in both the CHIKV-*nanoluc* spectrum and the CHIKV-*nanoluc*-compound **9** complex. This disappearance suggests additional interactions involving CH_2 wagging vibrations of phospholipids and in CO vibrations of polysaccharides, respectively.

4. Discussion

In this work, we evaluated the anti-CHIKV activity of 20 sulfonamide derivative compounds. These compounds have previously demonstrated potent and selective anti-ZIKV activity, highlighting their potential to inhibit other viruses [24]. All compounds were evaluated through cell viability and antiviral activity employing BHK-21 cells and CHIKV expressing the *nanoluciferase* reporter.

From investigated compounds, 17 exhibited statistically significant inhibition of CHIKV replication, although compounds **6**, **9**, **11**, and **13** presented the highest replication inhibition rates (more than 80% at 10 µM for **6**, **9,** and **11**, and 50 µM for **13**), demonstrating a dose–response activity against CHIKV with EC_{50} of 14.9, 17.0, 63.1, and 41.6 µM and SIs of 13.8, 5.8, 4.4, and 11.0, respectively.

Carboxylic acid-derived sulfonamide compounds (**14–20**) exhibited the weakest inhibition of CHIKV replication (Figure 2(d)), suggesting that heteroaromatic moiety is crucial for antiviral efficacy. Furthermore, all four of the most potent compounds (**6**, **9**, **11**, and **13**) are BTA derivatives, highlighting the significance of this scaffold in antiviral activity.

Compounds **6** and **9** were identified as the most potent compounds, exhibiting EC_{50} values of 14.9 and 17.0 µM, respectively. The key structural difference between these two compounds lies in the position, type, and number of substituents on the benzenesulfonyl ring. Specifically, compound **6** features a methyl group at the 4-position, while compound **9** possesses a methoxy group at the 2-position and a chlorine atom at the 5-position. Compounds bearing non-electron-donating substituents (**4**, **5**, and **10**) demonstrated limited efficacy in inhibiting CHIKV replication at non-cytotoxic concentrations, suggesting the importance of electron-donating groups for anti-CHIKV activity. However, compound **8**, an analog of **9** where chlorine is replaced with a methoxy group, exhibited lower efficacy than **9**, despite possessing two electron-donating substituents on the benzenesulfonyl ring. These findings, along with the reduced activity against CHIKV observed for compounds with more significant structural modifications, underscore the potential for subtle chemical variations to modulate interactions with CHIKV. Nevertheless, a comprehensive SAR study involving a broader range of chemical diversity is warranted to further elucidate these relationships.

In addition, it was shown through time-of-drug-addition assay that **6**, **9**, **11**, and **13** possess strong activity on post-entry stage. Furthermore, **9** demonstrated activity on all stages of the CHIKV replicative cycle investigated here.

The production of synthetic compounds from the skeleton of organic molecules has demonstrated relevant advantages, such as ease of large-scale production, the possibility of patenting and the improvement of bioactivity, and increasing specificity for certain targets. Through the structure–activity relationship (SAR) commonly applied in medicinal chemistry, BTA derivatives have shown to possess strong antiviral properties, acting as allosteric inhibitors of NS2A/NS3 proteases of DENV [21] and ZIKV [34], NS3 and NS5B of HCV [35,36], and the reverse transcriptase of HIV [37]. Similarly, our group demonstrated the action of **9** against ZIKV *in vitro*, those with BTA insertions [24]. Consequently, a direct comparison of antiviral effects against ZIKV and CHIKV is limited to **9** and **11**, for which EC_{50} values were determined against both viruses. Compound **9** exhibited comparable activity against both viruses, with EC_{50} values of 17 µM against CHIKV and 10.7 µM against ZIKV. In contrast, **11** demonstrated a significant difference in potency, showing an EC_{50} of 63.1 µM against CHIKV and 5.1 µM against ZIKV, indicating approximately 12-fold greater potency against ZIKV. Furthermore, **1** and **5** displayed EC_{50} values of 5 µM against ZIKV but were not selected for EC_{50} determination against CHIKV due to inhibition below 80% at non-cytotoxic concentrations. Given the limited data

available for a comprehensive direct comparison, it is challenging to draw definitive conclusions regarding the structural features conferring viral selectivity. However, the observed differences among **1**, **5**, **9**, and **11** suggest that subtle structural variations can significantly modulate antiviral activity against both ZIKV and CHIKV. Notably, ZIKV appears to exhibit greater sensitivity to this BTA class of compounds.

The strongest effects observed for all derivatives were in the post-entry stage of CHIKV replicative cycle, suggesting that the interference of CHIKV replication could be related to the replicative complex of CHIKV nsPs. In this context, the molecular docking calculations performed here corroborate this hypothesis. Each of these nsPs plays many roles in virus replication, assembled into a viral replicative complex, fundamental for CHIKV genome replication and transcription [38]. The nsP1 possesses capping attributes, functioning as both a methyltransferase and guanylyltransferase; nsP2 operates as RNA triphosphatase, nucleoside triphosphatase (NTPase), and RNA helicase; nsP3 is a multifunctional protein involved in several processes of recruiting host cell factors to improve viral replication, participates in the formation of replicative sites and modulates host immune response; and, ultimately, nsP4 is a key enzyme to the replicative process, known as RNA-dependent-RNA polymerase, responsible mainly for catalyzing genome elongation [39–41].

In contrast, **9** was capable of interfering with all the stages of CHIKV replication cycle investigated. The results obtained here corroborate our previous published findings with ZIKV. However, in the experiments conducted with the BHK-ZIKV replicon, **9** did not show a significant inhibition, indicating that its mode of action might not be exclusively related to the nsPs [24]. The molecular interactions between the compound **9** and CHIKV-*nanoluc* detected at 3040 cm^{-1} suggest interactions related to the stretching of C–H in the lipid membrane of the virus. These lipidic interactions could explain the virucidal effect of this compound, given that CHIKV is an enveloped virus surrounded by a bilipid layer derived from the host cell, as well as may justify the inhibition observed at the entry stage [42]. Additionally, CHIKV replicates into lipidic membranes' structures that could also be affected by this compound, disrupting the replication complex [43].

Our FTIR analysis provided further insights into the interaction between compound 9 and CHIKV. Notably, the second derivative spectra revealed the emergence of a distinct vibrational band at 3040 cm^{-1} in the CHIKV + 9 spectrum which was absent in the spectra of compound 9 or CHIKV alone. This spectral feature suggests that compound 9 may be interacting with CHIKV through C–H stretching vibrations, possibly involving lipid components of the viral envelope. Additionally, characteristic vibrational bands of compound 9 at 1269 cm^{-1} and 1018 cm^{-1} were absent in the CHIKV + 9 spectrum, indicating that compound 9 may be interacting with functional groups within this region, likely involving CH_2 wagging vibrations of phospholipids and CO vibrations of polysaccharides. These findings align with previous studies on FTIR spectral variations in biological macromolecules [33]. These structural insights further reinforce the potential of compound 9 as a promising antiviral candidate against CHIKV.

5. Conclusion

The data presented here demonstrate that BTA derivatives exhibit anti-CHIKV activity by inhibiting some points of its replicative cycle *in vitro*. In this regard, these compounds represent templates for the development of potential new drug candidates against CHIKF, highlighting the importance of synthesizing molecules based on improving their pharmacological and pharmacokinetic properties. While the *in vitro* results provide evidence and mechanistic insights through molecular docking and spectroscopy, additional investigations in physiologically relevant models will be valuable to complement these findings. Future research may focus on evaluating the pharmacokinetic behavior, *in vivo* antiviral efficacy, and potential host–virus interaction dynamics of these compounds, as well as on refining their structures to enhance selectivity and potency.

Funding

SFL and NMC thanks Coordenação de Aperfeiçoamento de Pessoal de Nível Superior (CAPES), scholarships [#703845/2022–00 and #88887.703841/2022–00], respectively. ACGJ is grateful to CAPES-Brazil-Prevention and Combat of Outbreaks, Endemics, Epidemics and Pandemics-Finance Code [#88881.506794/2020–01]. ACGJ is also grateful to FAPEMIG (Minas Gerais Research Foundation [APQ-01487-22 and APQ-04686-22] and CAPES-Finance Code 001 and Conselho Nacional de Desenvolvimento Científico e Tecnológico (CNPq) – Finance code [409187/2023–2].

Declaration of competing interest

The authors have no relevant affiliations or financial involvement with any organization or entity with a financial interest in or financial conflict with the subject matter or materials discussed in the manuscript. This includes employment, consultancies, honoraria, stock ownership or options, expert testimony, grants or patents received or pending, or royalties.

Authors contributions

Conceptualization: SFL, ACGJ, CORJ; **Data curation**: SFL, NMC, UAER, RFCD, DNF, MGV, NNJ; **Formal analysis**: SFL; **Funding acquisition**: ACGJ; **Investigation**: SFL; **Project Administration**: ACGJ; **Supervision**: ACGJ; **Validation**: ACGJ; **Visualization**: SFL; **Writing – original draft**: SFL; **Writing – review and editing**: NMC, RSS, CORJ, ACGJ.

Acknowledgments

We thank Andres Merits (Institute of Technology, University of Tartu, Tartu, Estonia) for the provision of the CHIKV expressing-nanoluciferase.

References

Papers of special note have been highlighted as either of interest (•) or of considerable interest (••) to readers.

1. Burt FJ, Rolph MS, Rulli NE, et al. Chikungunya: a re-emerging virus. Lancet [Internet]. 2012 [cited 2024 Mar 10];379(9816):662–671. doi: 10.1016/S0140-6736(11)60281-X

• **This article provides a comprehensive overview of Chikungunya virus (CHIKV) pathogenesis, epidemiology, and immune responses, making it a key reference for understanding the virus's resurgence.**

2. Montalvo Zurbia-Flores G, Reyes-Sandoval A, Kim YC. Chikungunya virus: priority pathogen or passing trend? Vaccines (Basel) [Internet]. 2023 [cited 2024 Mar 10];11(3):568. doi: 10.3390/vaccines11030568
3. de Souza WM, Ribeiro GS, de Lima STS, et al. Chikungunya: a decade of burden in the Americas. Lancet Reg Health - Am [Internet]. 2024 [cited 2024 Mar 10];30:100673. doi: 10.1016/j.lana.2023.100673
4. Ahmed Imad H, Phadungsombat J, Nakayama EE, et al. Clinical features of acute chikungunya virus infection in children and adults during an outbreak in the Maldives. 2021 [cited 2024 Mar 10]. doi: 10.4269/ajtmh.21-0189
- **This paper reviews the public health burden of CHIKV in the Americas over the past decade, providing critical insights into epidemiological trends and disease impact.**
5. Philip. Why synthesize? 2015.
6. Sáenz-Galindo A, Castañeda-Facio AO, Cedillo-Portillo JJ, et al. Beyond the molecular frontier: challenges for chemistry and chemical engineering. National Academies Press; 2020 [cited 2024 Mar 16]. p. 283–291.
7. Gaffer HE, Mahmoud SA, El-Sedik MS, et al. Synthesis, molecular modelling, and antibacterial evaluation of new sulfonamide-dyes based pyrrole compounds. Sci Rep [Internet]. 2024 [cited 2024 Jul 6];14(1):1–17. doi: 10.1038/s41598-024-60908-8
- **This paper explores the design and synthesis of sulfonamide-based compounds with potential antibacterial applications, providing insights into structural modifications relevant to drug discovery.**
8. Kalay E. Synthesis and characterization of novel hybrid sulfonamide molecules with benzothiazole scaffold. Iğdır Üniversitesi Fen Bilimleri Enstitüsü Dergisi [Internet]. 2022 [cited 2024 Jul 6];12(2):899–907. doi: 10.21597/jist.1039476
9. Nguyen VT, Haug GC, Nguyen VD, et al. Photocatalytic decarboxylative amidosulfonation enables direct transformation of carboxylic acids to sulfonamides. Chem Sci [Internet]. 2021 [cited 2024 Jul 9];12(18):6429–6436. doi: 10.1039/D1SC01389K
10. Wan Y, Fang G, Chen H, et al. Sulfonamide derivatives as potential anti-cancer agents and their SARs elucidation. Eur J Med Chem. 2021;226:113837. doi: 10.1016/j.ejmech.2021.113837
11. Irfan A, Batool F, Andleeb S, et al. Benzothiazole derivatives as anticancer agents. [cited 2024 Mar 10]. doi: 10.1080/14756366.2019.1698036
- **This paper discusses the anticancer potential of benzothiazole derivatives, offering structural insights that could be relevant to antiviral drug development.**
12. Le Bozec L, Moody CJ. Naturally occurring nitrogen–sulfur compounds. The benzothiazole alkaloids. Aust J Chem [Internet]. 2009 [cited 2024 Jul 5];62(7):639–647. doi: 10.1071/CH09126
13. Asiri YI, Alsayari A, Muhsinah AB, et al. Benzothiazoles as potential antiviral agents. 2020 [cited 2024 Mar 16]. doi: 10.1111/jphp.13331
14. Cai J, Sun M, Wu X, et al. Design and synthesis of novel 4-benzothiazole amino quinazolines dasatinib derivatives as potential anti-tumor agents. Eur J Med Chem. 2013;63:702–712. doi: 10.1016/j.ejmech.2013.03.013
15. Meltzer-Mats E, Babai-Shani G, Pasternak L, et al. Synthesis and mechanism of hypoglycemic activity of benzothiazole derivatives. J Med Chem [Internet]. 2013 [cited 2024 Jun 28];56(13):5335–5350. doi: 10.1021/jm4001488
16. None S, K A, M AK. Advancement in pharmacological activities of benzothiazole and its derivatives: an up to date review. Mini Rev Med Chem [Internet]. 2021 [cited 2024 Mar 10];21(3):314–335. doi: 10.2174/1389557520666200820133252
17. Lapierre TJWJD, Farago DN, de Moura Lodi Cruz MGF, et al. Evaluation and discovery of novel benzothiazole derivatives as promising hits against leishmania infantum. Chem Biol Drug Des [Internet]. 2024 [cited 2024 Jul 1];103(4):e14525. doi: 10.1111/cbdd.14525
18. Zhu W, Liu F, Yu B, et al. Preparation of antibacterial acrylic bone cement with methacrylate derived from benzothiazole. J Mech Behav Biomed Mater [Internet]. 2021 [cited 2024 Mar 10];117:104403. doi: 10.1016/j.jmbbm.2021.104403
19. Abdel-Aziza HA, Abdel-Wahab BF, Badria FA. Stereoselective synthesis and antiviral activity of (1E,2Z,3E)-1-(piperidin-1-yl)-1-(arylhydrazono)-2-[(benzoyl/benzothiazol- 2-oyl)hydrazono]-4-(aryl1)but-3-enes. Arch Pharm (Weinheim) [Internet]. 2010 [cited 2024 Jun 28];343(3):152–159. doi: 10.1002/ardp.200900195
20. Galochkina AV, Bollikanda RK, Zarubaev VV, et al. Synthesis of novel derivatives of 7,8-dihydro-6H-imidazo[2,1-b][1,3]benzothiazol-5-one and their virus-inhibiting activity against influenza a virus. Arch Pharm (Weinheim) [Internet]. 2019 [cited 2024 Jun 28];352(2):1800225. doi: 10.1002/ardp.201800225
21. Wu H, Bock S, Snitko M, et al. Novel dengue virus NS2B/NS3 protease inhibitors. Antimicrob Agents Chemother [Internet]. 2015 [cited 2024 Mar 17];59(2):1100–1109. doi: 10.1128/AAC.03543-14
22. Ivasiv V, Albertini C, Gonçalves AE, et al. Molecular hybridization as a tool for designing multitarget drug candidates for complex diseases. Curr Top Med Chem [Internet]. 2019 [cited 2024 Jul 6];19(19):1694–1711. doi: 10.2174/1568026619666190619115735
23. Sandhu S, Bansal Y, Silakari O, et al. Coumarin hybrids as novel therapeutic agents. Bioorg Med Chem. 2014;22(15):3806–3814. doi: 10.1016/j.bmc.2014.05.032
24. Dias RFC, Ribeiro BMRM, Cassani NM, et al. Discovery and structural optimization of a new series of N-acyl-2-aminobenzothiazole as inhibitors of Zika virus. Bioorg Med Chem [Internet]. 2023 [cited 2023 Nov 1];95:117488. doi: 10.1016/j.bmc.2023.117488
- **This research is the one that we based all our work. In this we showed details of the optimization of our derivatives, but with a structural-hit design for Zika virus.**
25. Matkovic R, Bernard E, Fontanel S, et al. The host DHX9 DExH-box helicase is recruited to chikungunya virus replication complexes for optimal genomic RNA translation. J Virol [Internet]. 2019 [cited 2023 Mar 3];93(4). doi: 10.1128/JVI.01764-18
26. Andrade Santos I, Farinha Shimizu J, Moraes de Oliveira D, et al. Chikungunya virus entry is strongly inhibited by phospholipase A2 isolated from the venom of Crotalus durissus terrificus. Sci Rep [Internet]. [cited 2024 Apr 22];11(1):8717. doi: 10.1038/s41598-021-88039-4
27. Mirdita M, Schütze K, Moriwaki Y, et al. ColabFold: making protein folding accessible to all. Nat Methods [Internet]. 2022 [cited 2024 Mar 28];19(6):679. doi: 10.1038/s41592-022-01488-1
28. Meng EC, Goddard TD, Pettersen EF, et al. UCSF chimeraX: tools for structure building and analysis. Protein Sci. 2023;32(11). doi: 10.1002/pro.4792
29. Grosche VR, Souza LPF, Ferreira GM, et al. Mannose-binding lectins as potent antivirals against SARS-CoV-2. Viruses [Internet]. 2023 [cited 2024 Jul 1];15(9):1886. doi: 10.3390/v15091886
30. Ruiz UEA, Santos IA, Grosche VR, et al. Imidazonaphthyridine effects on chikungunya virus replication: antiviral activity by dependent and independent of interferon type 1 pathways. Virus Res. 2023;324:199029. doi: 10.1016/j.virusres.2022.199029
31. Rieppo L, Saarakkala S, Närhi T, et al. Application of second derivative spectroscopy for increasing molecular specificity of Fourier transform infrared spectroscopic imaging of articular cartilage. Osteoarthritis Cartilage [Internet]. 2012 [cited 2025 Apr 25];20(5):451–459. doi: 10.1016/j.joca.2012.01.010
32. Cassani NM, Santos IA, Grosche VR, et al. Roles of Bothrops jararacussu toxins I and II: antiviral findings against Zika virus. Int J Biol Macromol. 2023;227:630–640. doi: 10.1016/j.ijbiomac.2022.12.102
33. Movasaghi Z, Rehman S, Rehman IU. Fourier transform infrared (FTIR) spectroscopy of biological tissues. Appl Spectrosc Rev. 2008;43(2):134–179. doi: 10.1080/05704920701829043
34. Maus H, Barthels F, Hammerschmidt SJ, et al. SAR of novel benzothiazoles targeting an allosteric pocket of DENV and ZIKV NS2B/NS3 proteases. Bioorg Med Chem. 2021;47:116392. doi: 10.1016/j.bmc.2021.116392

35. Li K, Frankowski KJ, Belon CA, et al. Optimization of potent hepatitis C virus NS3 helicase inhibitors isolated from the yellow dyes thioflavine S and primuline. J Med Chem [Internet]. 2012 [cited 2024 Jul 5];55(7):3319–3330. doi: 10.1021/jm300021v
36. Manfroni G, Meschini F, Barreca ML, et al. Pyridobenzothiazole derivatives as new chemotype targeting the HCV NS5B polymerase. Bioorg Med Chem. 2012;20(2):866–876. doi: 10.1016/j.bmc.2011.11.061
37. Akbay A, Ören I, Temiz-Arpaci Ö, et al. Synthesis and HIV-1 reverse transcriptase inhibitor activity of some 2,5,6-substituted benzoxazole, benzimidazole, benzothiazole and oxazolo (4,5-b)pyridine derivatives. Arzneimittel-Forsch/Drug Res. 2003;53(4):266–271. doi: 10.1055/s-0031-1297107
38. Bartholomeeusen K, Utt A, Coppens S, et al. A chikungunya virus trans -replicase system reveals the importance of delayed nonstructural polyprotein processing for efficient replication complex formation in mosquito cells. J Virol [Internet]. 2018 [cited 2024 Jun 23];92(14):152–170. doi: 10.1128/JVI.00152-18
39. Freire MCLC, Basso LGM, Mendes LFS, et al. Characterization of the RNA-dependent RNA polymerase from Chikungunya virus and discovery of a novel ligand as a potential drug candidate. Sci Rep [Internet]. 2022 [cited 2024 Jun 23];12(1):1–15. doi: 10.1038/s41598-022-14790-x
- **This paper provides an extensive review of antiviral strategies targeting CHIKV, discussing both direct-acting antivirals and host-directed therapies. The CHIKV nsP4 direct-act approach highlights the importance in addressing the virus RNA dependent RNA polymerase as an antiviral strategy as found in our molecular docking results with compound 9.**
40. Schwartz O, Albert ML. Biology and pathogenesis of chikungunya virus. Nat Rev Microbiol [Internet]. 2010 [cited 2024 Jun 23];8(7):491–500. doi: 10.1038/nrmicro2368
- **This study describes the assembly of alphavirus replication complexes, providing fundamental insights into viral RNA synthesis and replication mechanisms, highlighting the importance of targeting lipids as an antiviral alternative.**
41. Subudhi BB, Chattopadhyay S, Mishra P, et al. Current strategies for inhibition of chikungunya infection. Viruses [Internet]. 2018 [cited 2024 Jun 23];10(5):235. doi: 10.3390/v10050235
42. Caglioti C, Lalle E, Castilletti C, et al. Chikungunya virus infection: an overview. New Microbiologica. 2013;36(3):211–227.
43. Spuul P, Balistreri G, Hellström K, et al. Assembly of alphavirus replication complexes from RNA and Protein components in a novel trans -replication system in mammalian cells. J Virol [Internet]. 2011 [cited 2024 Jul 5];85(10):4739–4751. doi: 10.1128/JVI.00085-11